Science of the Total Environment xxx (2016) xxx–xxx

Contents lists available at ScienceDirect

Science of the Total Environment

journal homepage: www.elsevier.com/locate/scitotenv

Chemical and physical properties of biomass burning aerosols and their CCN activity: A case study in Beijing, China

Zhijun Wu *, Jing Zheng, Yu Wang, Dongjie Shang, Zhoufei Du, Yuanhang Zhang, Min Hu *

State Key Joint Laboratory of Environmental Simulation and Pollution Control, College of Environmental Sciences and Engineering, Peking University, Beijing 100871, China

HIGHLIGHTS

- A clear burst and continuous growth of ultrafine particles occurred during biomass burning episode.
- Organics and black carbon (BC) were dominant in the biomass-burning aerosols, accounting for 60 ± 10% and 18 ± 3% of PM_1.
- The κ values of biomass burning aerosols converged to 0.1 and did not show high variability.

GRAPHICAL ABSTRACT

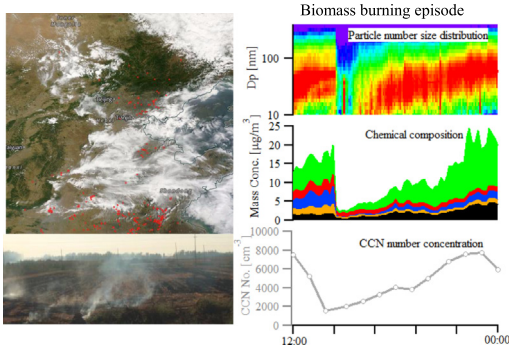

ARTICLE INFO

Article history:
Received 29 August 2016
Received in revised form 14 November 2016
Accepted 17 November 2016
Available online xxxx

Editor: D. Barcelo

Keywords:
Biomass burning
Hygroscopicity
CCN
Chemical composition

ABSTRACT

Biomass burning emits large amounts of both trace gases and particles into the atmosphere. It plays a profound role in regional air quality and climate change. In the present study, an intensive campaign was carried out at an urban site in Beijing, China, in June 2014, which covered the winter wheat harvest season over the North China Plain (NCP). Meanwhile, two evident biomass-burning events were observed. A clear burst in ultrafine particles (below 100 nm in diameter, PM_1) and subsequent particle growth took place during the events. With the growth of the ultrafine particles, the organic fraction of PM_1 increased significantly. The ratio of oxygen to carbon (O:C), which had an average value of 0.23 ± 0.04, did not show an obvious enhancement, indicating that a significant chemical aging process of the biomass-burning aerosols was not observed during the course of events. This finding might have been due to the fact that the biomass-burning events occurred in the late afternoon and grew during the nighttime, which is associated with a low atmospheric oxidation capacity. On average, organics and black carbon (BC) were dominant in the biomass-burning aerosols, accounting for 60 ± 10% and 18 ± 3% of PM_1. The high organic and BC fractions led to a significant suppression of particle hygroscopicity. Comparisons among hygroscopicity tandem differential mobility analyzer (HTDMA)-derived, cloud condensation nuclei counter (CCNc)-derived, and aerosol mass spectrometer-based hygroscopicity parameter (κ) values were consistent. The mean κ values of biomass-burning aerosols derived from both HTDMA and CCNc measurements were approximately 0.1, regardless of the particle size, indicating that the biomass-burning aerosols were less active. The burst in particle count during the biomass-burning events resulted in an increased number of cloud condensation nuclei (CCN) at supersaturation (SS) = 0.2–0.8%.

* Corresponding authors.
E-mail addresses: zhijunwu@pku.edu.cn (Z. Wu), minhu@pku.edu.cn (M. Hu).

http://dx.doi.org/10.1016/j.scitotenv.2016.11.112
0048-9697/

1. Introduction

Globally, open biomass burning emits 2800 Gg year^{-1} black carbon (BC) and contributes to one-third of the global BC budget (Bond et al., 2013). Biomass burning is also a major source of organic aerosols, contributing to two-thirds of the global primary organic aerosol budget (Bond et al., 2013). BC in the atmosphere has a significant effect on the global and regional climate directly by absorbing solar radiation and indirectly by serving as cloud condensation nuclei (CCN) (Andreae and Rosenfeld, 2008). Atmospheric modeling has shown that biomass burning is an important global source of CCN (Spracklen et al., 2011). Some evidence has shown that organic aerosols emitted from biomass burning contain substantial amounts of light-absorbing brown carbon, which is a non-negligible contributor to positive direct aerosol radiative forcing (Chen and Bond, 2010; Saleh et al., 2014). Currently, the climatic effects of biomass-burning particles have remained poorly quantified due to very high variability in the optical and CCN-activating properties of biomass-burning aerosols (Bond et al., 2013; Vakkari et al., 2014).

Biomass burning emits large amounts of trace gases and particles into the atmosphere (Andreae and Merlet, 2001). As the biomass-burning plume is transported away from the fire, atmospheric dilution and photochemical oxidation rapidly transform the gaseous and particulate emissions (Robinson et al., 2010; Trentmann et al., 2003; Vakkari et al., 2014). Studies in both field and laboratory experiments have shown that changes in the size distribution, hygroscopicity, and chemical composition of biomass-burning particles take place during their atmospheric transport (Capes et al., 2008; Hennigan et al., 2012; Reid et al., 2005). The overall picture of these changes has remained heterogeneous.

The North China Plain (NCP) is the major region for planting winter wheat in China. During the months of May and June, burning straw waste in the winter wheat fields emits large amounts of aerosol particles and trace gases into the atmosphere, giving rise to a deteriorated air quality that causes adverse effects on human health in adjacent cities (Cheng et al., 2013; Duan et al., 2004; Mukai et al., 2014). In our study, an intensive campaign was carried out to measure the air quality in Beijing, China, in June 2014, which covered the intensive biomass-burning period in the NCP regions. During the field campaign, the biomass-burning episodes caused bursts in ultrafine particles and subsequent growth. Herein, we provide a picture of the chemical and physical properties of the ultrafine particles produced during the biomass-burning episodes by integrating the measurements of particle size distribution, chemical composition, and particle hygroscopicity. Additionally, the CCN activity of ultrafine particles during biomass-burning episodes was evaluated.

2. Experiments

The intensive field campaign was carried out in June 2014 in Beijing, China. The sampling site was on the roof of a six-floor building (about 30 m above ground level) on the campus of Peking University (39°59′20″N, 116°18′26″E), located in the northwestern urban area of Beijing. At the sampling site, meteorological parameters including wind speed, wind direction, relative humidity (RH), and temperature were measured by a weather station. Gaseous pollutants were continuously measured by Thermo Environmental Instruments (O_3 (Model 49i) and CO (Model 48i TLE)).

The instruments used for aerosol measurements were installed in a well-air-conditioned laboratory. The RH of the sampled air was kept below 30% using a silica gel dryer and a Nafion dryer, in series. The detailed measurement descriptions of the chemical and physical properties of the particles are given below.

2.1. Particle chemical composition

An Aerodyne high-resolution-time-of-flight aerosol mass spectrometer (here simply referred to as AMS) (DeCarlo et al., 2006) was operated in "mass spectrum" and "particle-time-of-flight" submodes for equal time periods. Due to the 600 °C surface temperature of the vaporizer, the AMS can only analyze the nonrefractory chemical composition of the particles. Elemental carbon, crustal material, and sea salt cannot be detected. Therefore, based on the transmission efficiency of the aerodynamic lenses and the detected compounds, the AMS can provide the size-resolved chemical composition of the submicrometer nonrefractory aerosol particle fraction (NR-PM_1) (Canagaratna et al., 2007). Applying the method developed by Canagaratna et al. (2015), the high-resolution organic particle mass spectra were used to determine the elemental composition and the oxygen to carbon atomic ratio (O:C). The particle diameter detected by AMS was converted to the particle mobility diameter by division of the AMS vacuum aerodynamic diameter by the estimated particle density. Here, particle density was estimated by comparing the mass-diameter distributions derived from the AMS measurements and the particle volume distributions calculated from the scanning mobility particle sizer (SMPS) measurements, as described previously by Kostenidou et al. (2007) and Chen et al. (2012). Here, we assumed that the particles detected with a shape factor of 1 are spherical. The particle volume size distribution was calculated from the particle size distribution. The optimized particle effective density was 1520 kg/m^3. Hereafter, the mobility diameter (assuming spherical particles) was used for the AMS data below.

The BC mass concentration in μg/m^3 was derived from a Photoacoustic Extinctiometer (PAX) (DMT Company) (Arnott et al., 1999) equipped with a PM_1 cut-off inlet. In this study, PAX measurements were performed at a wavelength of 532 nm. Before carrying out the PAX measurements, the device was calibrated carefully using lab-generated monodisperse polystyrene latex particles and polydisperse propane soot particles. The calibration curves were used to correct the measured scattering and absorption coefficients.

2.2. Particle hygroscopicity measurements

The hygroscopicity tandem differential mobility analyzer (HTDMA) used in this study has been illustrated in previous publications in detail (Massling et al., 2003; Wu et al., 2011) and complied with the instrumental standards prescribed by Massling et al. (2011). The HTDMA consists of three main parts: (1) a differential mobility analyzer (DMA1) that selects quasi-monodisperse particles and a condensation particle counter (CPC1) that measures the number of particles leaving the DMA1 at the selected particle size; (2) an aerosol humidifier conditioning the particles selected by DMA1 to a defined RH; (3) a second differential mobility analyzer (DMA2) coupled with another condensation particle counter (CPC2) to measure the size distributions of the humidified aerosol. DMA2 and the aerosol humidifier were placed in a temperature-controlled box. Hygroscopicity scans with 100-nm ammonium sulfate particles were performed frequently to analyze the stability of the RH set at 90% in DMA2. Hygroscopicity scans with a deviation of >3% in RH to the set-point of 90% were not considered for further analysis.

The hygroscopic growth factor (HGF) was defined as the ratio of the particle mobility diameter, $D(RH)$, at a given RH to the dry diameter, D_d:

$$\mathrm{HGF(RH)} = \frac{D(RH)}{D_d} \quad (1)$$

The TDMA*inv* method developed by Gysel et al. (2009) was used to invert the HTDMA data. Dry scans (RH < 10%) were used to calibrate a possible offset between DMA1 and DMA2 and to define the width of the HTDMA's transfer function (Gysel et al., 2009). The growth factor probability density function (GF-PDF) was derived from TDMAinv. The GF-PDF values measured in the range of 87% < RH < 93% were corrected to RH = 90%.

Please cite this article as: Wu, Z., et al., Chemical and physical properties of biomass burning aerosols and their CCN activity: A case study in Beijing, China, Sci Total Environ (2016), http://dx.doi.org/10.1016/j.scitotenv.2016.11.112

The hygroscopicity parameter, κ, was calculated from the HGF measured by HTDMA (Petters and Kreidenweis, 2007) as follows:

$$\kappa_{HTDMA} = \left(HGF^3 - 1\right)\left(\frac{exp\left(\frac{A}{D_{Pdry}\cdot HGF}\right)}{RH} - 1\right) \quad (2)$$

$$A = \frac{4\sigma_{s/a}M_w}{RT\rho_w} \quad (3)$$

where D_{Pdry} and HGF are the initial dry particle diameter and the HGF at 90% RH measured by HTDMA, respectively, $\sigma_{s/a}$ is the droplet surface tension (assumed to be that of pure water, $\sigma_{s/a} = 0.0728$ N m^{-2}), M_w is the molecular weight of water, ρ_w is the density of liquid water, R is the universal gas constant, and T is the absolute temperature.

2.3. Particle size distributions and CCN measurements

Particle size distributions were measured by a SMPS spectrometer (Long Differential Mobility Analyzer (DMA) 3081, condensation particle counter (CPC) 3775, and nano-SMPS (Nano DMA 3085 + CUCPC 3776). The sheath flow rates for nano-SMPS and SMPS were 15 and 3 L min^{-1}, respectively. The ratio of the sample flow rate to the sheath air flow rate was 1:10 for both DMAs. Using a sample flow rate of 3 L min^{-1} in the Long DMA, the maximum particle size detected was 736 nm. In addition, multiple charge correction, CPC counting efficiency, and particle loss correction were carried out.

A Cloud Condensation Nucleus counter (CCNc DMT, USA; Roberts and Nenes, 2005) was coupled to a Hauke-type DMA and a CPC (TSI model 3010). Within the DMA, monodisperse particles can be selected. The aerosol flows after the DMA is split. One part is sent to a CPC, which counts the total number of aerosol particles. The other part is sent to the CCNc to count the activated particles at a certain supersaturation (SS). Afterwards, the activated fraction (AF) is determined, which is defined as the ratio of the activated particle count (CCN) to the total particle count at a particular SS. This is done for a certain diameter range to gain a full activation curve from zero activated particles up to full activation at an AF of one. This so-called diameter scan is corrected for double-charged particles (Deng et al., 2011) and afterwards fitted by a Gaussian error function:

$$AF = \frac{a+b}{2}\left[1 + erf\left(\frac{D - D_{50}}{\sigma\sqrt{2}}\right)\right] \quad (4)$$

where AF is the activated fraction, erf is the error function, D is the set diameter, D_{50} is the diameter at half of the maximum AF value, and σ is the standard deviation of the cumulative Gaussian distribution function. The center of the error function is interpreted as a critical diameter at a fixed SS. The hygroscopicity parameter, κ, can also be calculated from the critical diameter derived from CCNc measurements (Petters and Kreidenweis, 2007):

$$\kappa_{CCNc} = \frac{4A^3}{27D_{50}^3 ln^2 S_c} \quad (5)$$

where D_{50} is the critical diameter at which 50% of the particles are activated at SS, and S_c and A can be derived from Eq. (3).

3. Results and discussion

3.1. Burst and growth of ultrafine particles during the biomass-burning episodes

The wheat harvest season is normally from late May to early June over the NCP. During and after the harvest season, wheat straw waste is typically burned to fertilize the field. The NCP borders the Taihang Mountains in the west, the coast in the east, and the Yanshan Mountains in the north. Beijing is in the northwest part of the NCP. Under a prevailing south or southwest wind, Beijing can be a receptor for pollutants coming from biomass-burning plumes over the NCP. Several previous studies have already shown that wheat straw burning significantly contributes to degradation of air quality in Beijing during the harvest season (Li et al., 2008; Li et al., 2010; Wang et al., 2015; Zheng et al., 2005).

During our intensive campaign, two biomass-burning episodes were observed on June 7 and 8, 2014. As an example, the left panel of Fig. 1 displays moderate-resolution imaging spectroradiometry Terra + Aqua active fire hotspot detections on June 8. It indicates that widespread fires occurred over the NCP on this day. The air mass backward trajectory in the right panel of Fig. 1 shows that the air mass came from areas north of Beijing on June 7 and areas west of Beijing on June 8. The air mass moved slowly and had a transition from June 7 to 9. The

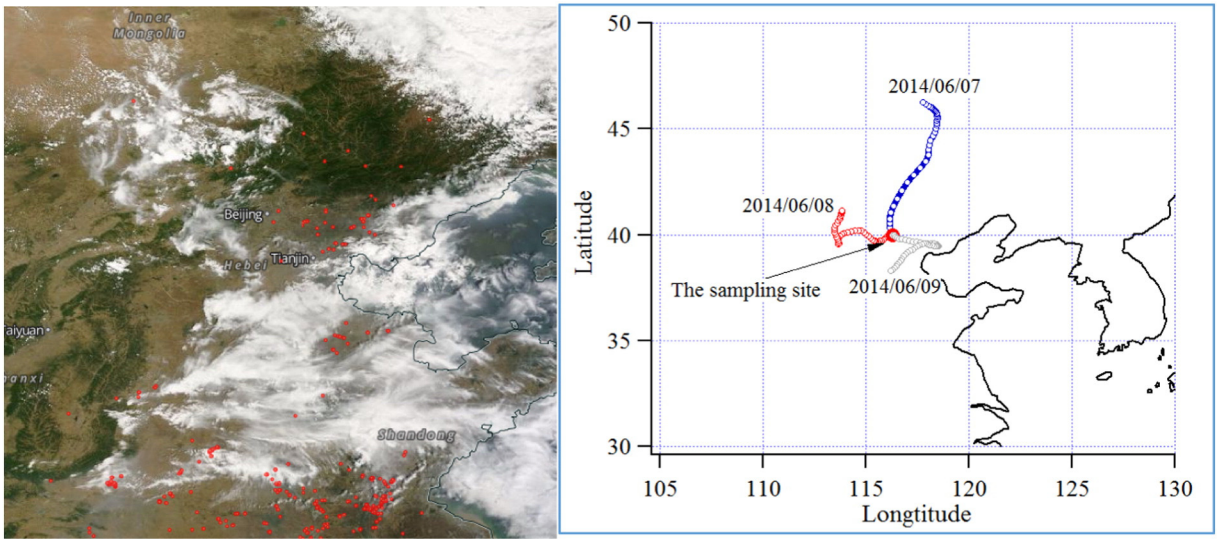

Fig. 1. (Left panel) Moderate-resolution imaging spectroradiometry Terra + Aqua active fire hotspot detections on June 8, 2014, over the North China Plain (https://worldview.earthdata.nasa.gov/) and (Right panel) airmass backward trajectories during biomass burning episode.

Please cite this article as: Wu, Z., et al., Chemical and physical properties of biomass burning aerosols and their CCN activity: A case study in Beijing, China, Sci Total Environ (2016), http://dx.doi.org/10.1016/j.scitotenv.2016.11.112

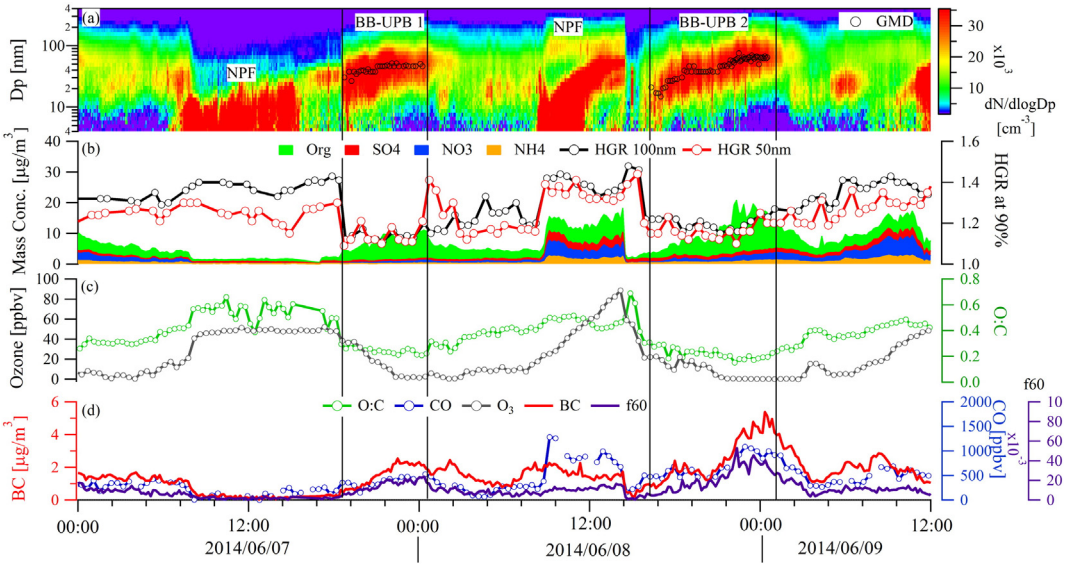

Fig. 2. Time course of particle size distribution, submicrometer nonrefractory aerosol particle fraction (NR-PM_1) chemical composition, hygroscopic growth factor (HGF), O:C ratio, f_{60}, and O_3, CO, and black carbon (BC) concentrations.

biomass burning that occurred in the surrounding areas of Beijing might have influenced the air mass in the sampling site; therefore, biomass-burning aerosols were detected.

Fig. 2 shows the time course of particle size distribution, chemical composition, ozone (O_3) concentration, O:C ratio, BC, m/z60 (f_{60}), and carbon monoxide (CO) concentration from June 7 to 9, 2014. The meteorological parameters are displayed in Fig. 3. Clearly, two typical new particle formation (NPF) events associated with the burst in the number of 3–10-nm particles were observed on June 7 and 8, as marked with "NPF" in Fig. 2. Similar to observations in previous studies (e.g. Wu et al., 2007), the NPF events started around 9:00 am and lasted several hours under dry conditions (Fig. 3b) and a low pre-existing particle concentration (Fig. 2b).

Between 14:00 and 16:00 on June 7, obvious changes in weather conditions occurred; as shown in Fig. 3, the air mass arriving at the sampling site changed. Similarly, the weather conditions changed and there was a brief shower around 14:00 on June 8. After the air mass changed, bursts in the Aitken mode particle count were observed on both June 7 and 8. Subsequently, the particles grew to larger sizes during the course of the event, as indicated by the geometric mean diameter (GMD) of the Aitken mode particles shown in Fig. 2. Different from the typical NPF events induced by photochemistry, these two events began in the late afternoon and started with a relatively larger particle size. Of note, the events took place when the RH was increasing and the temperature was decreasing, showing an opposite pattern to that when typical NPF events occur. In contrast to typical NPF events, a lower O_3 concentration was observed during the events. This evidence implied that the events had a different formation process from typical NPF events. Here, such events were defined as biomass burning-ultrafine particle burst (BB-UPB) events, which are marked with "BB-UPB 1 and BB-UPB 2" in Fig. 2. The two biomass-burning episodes were also validated by an enhanced CO concentration and f_{60}, which was derived from AMS measurements. The parameter f_{60}, which is a mass spectrometric biomass-burning tracer, is the ratio of signal at m/z 60 to the total signal of

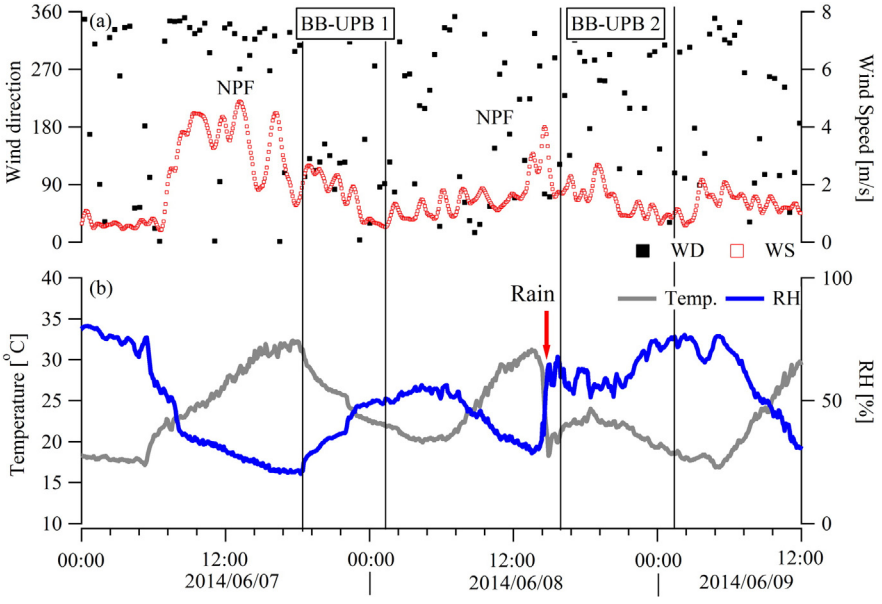

Fig. 3. Time course of wind speed (WS) and direction (WD), ambient temperature, and relative humidity (RH). BB-UPB 1 and BB-UPB 2 indicate biomass burning-ultrafine particle burst events 1 and 2, respectively. NPF indicates new particle formation.

Please cite this article as: Wu, Z., et al., Chemical and physical properties of biomass burning aerosols and their CCN activity: A case study in Beijing, China, Sci Total Environ (2016), http://dx.doi.org/10.1016/j.scitotenv.2016.11.112

organic matter. The dominate ion at m/z 60 corresponds to $C_2H_4O_2^+$, which is due to the fragmentation of levoglucosan (Cubison et al., 2011). Higher levels of f_{60} and CO were observed during the two plumes, compared to those of typical NPF events. This finding confirmed the observation of a biomass-burning plume.

As shown in Fig. 2a, the size distribution of biomass-burning particles was dominated by particles smaller than 200 nm. The GMD was 30–50 nm for the BB-UPB 1 event, and it was 20–90 nm for the BB-UPB 2 event. These values are smaller than those of most previous observations; the reported particle median diameter for fresh smoke is 0.10–0.16 μm, centered at 0.13 μm (Reid et al., 2005). The growth rates of BB-UPB 1 and 2 were 3.9 nm/h and 6.5 nm/h, respectively, as calculated by the changes in GMDs with time (ΔGMD/Δt). The ultrafine particles observed at the sampling site during the BB-UPB events may have been produced when the biomass-burning plume was transported away from the fire. One possibility is that the oxidation of the trace gases emitted from biomass burning produced low-volatility condensable vapors, which nucleated in the biomass-burning plume. A previous study has shown that exposing the exhaust from biomass burning to UV light initiates photochemistry in an environmental chamber, thus creating a strong nucleation burst and increasing the particle count significantly (Hennigan et al., 2012). After nucleation, the condensation of condensable vapors and coagulation lead to subsequent particle growth. As shown in Fig. 3b, the ambient temperature decreased significantly during the particle growth processes. A lower temperature facilitated the condensation of semi-volatile organic vapors onto the particles. Another possibility is that ultrafine particles could also be emitted directly by biomass burning and grew via condensation, coagulation, and chemical aging during transportation.

3.2. Chemical characterization of biomass-burning aerosols

As shown in Fig. 2b, an obvious enhancement of organic compound and BC mass concentrations was observed as the concentration of CO, a biomass-burning marker, increased. Increasing organics and BC mass concentrations in the air mass influenced by open-air biomass burning have been reported by many previous studies (Adler et al., 2011; Corrigan et al., 2013; Jung et al., 2014). Such enhancements of organics and BC as well as the simultaneous reduction in inorganic components (sulfate, ammonium, and nitrate) in biomass-burning particles were associated with significant suppression of particle hygroscopicity, as shown in Fig. 2b. Of note, the aerosols measured at our sampling site during biomass-burning episodes were not pure biomass-burning aerosols. This is because the sampling site is not close to the biomass-burning point. During transportation, changes in the biomass-burning aerosols, for example, mixed with urban aged aerosols, took place. On average, the organics and BC accounted for 60 ± 10% and 18 ± 3% of PM_1 during the BB-UPB episodes, respectively. Here, PM_1 means the sum of NR-PM_1 and BC mass concentrations. This result was similar to those reported in previous studies. For example, Reid et al. (2005) compiled the existing observations on biomass-burning emissions in the literature and showed that biomass-burning aerosols are composed of 50–60% organic carbon and 5–10% BC. Recently, Bougiatioti et al. (2014) observed that biomass-burning aerosols transported several hundreds of kilometers consisted of 46.5% organics and 9.5% BC in terms of mass concentration.

During the BB-UPB episodes, the average O:C ratio was 0.23 ± 0.04, which is in the range of the O:C ratio (from 0.18 to 0.26) of organic aerosols from fresh-biomass-burning emissions (He et al., 2010). The oxidation state of organics increases with time (Adler et al., 2011). However, as displayed in Fig. 2c, no increasing trend of the O:C ratio was observed during the course of the BB-UPB events, indicating that the chemical aging of biomass-burning aerosols was insignificant. This result is due to the fact that the BB-UPB events occurred in the late afternoon and grew during the nighttime, which is associated with a low atmospheric oxidation capacity. The mean O_3 concentrations were 14 and 9 ppbv for biomass-burning episodes 1 and 2, respectively, proving that the photochemical activity was very weak during this period.

The particle mass size distributions of sulfate (SO_4^{2-}), nitrate (NO_3^-), and ammonium (NH_4^+) ions as well that of organic compounds (Org) derived from averaging the AMS data over the BB-UPB time periods are shown Fig. 4. The organic compounds were the dominant fraction, independent of particle size. Its mass concentration peaked at approximately 250 nm in diameter. The inorganic fraction was insignificant. As indicated by the particle size distribution (Fig. 2), the particles were mainly smaller than 200 nm in diameter during the BB-UPB episodes. The size distribution of the mass concentration showed that those particles mainly consisted of organics.

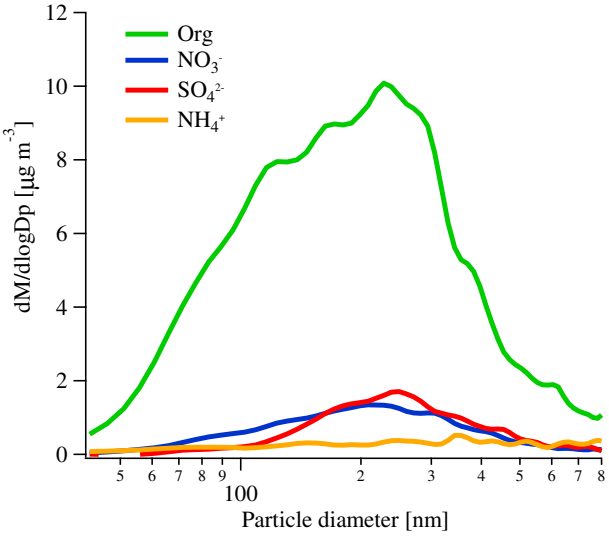

Fig. 4. Particle mass size distribution of chemical species in biomass-burning aerosols.

3.3. Particle hygroscopicity during the BB-UPB events

Fig. 5 shows the time course of GF-PDF for 50-, 100-, and 250-nm particles as well as the particle number fraction of hydrophobic mode. Here, particles with HGF < 1.2 were considered as hydrophobic mode, while those with HGF > 1.2 were hydrophilic mode. The GF-PDFs for all selected particle sizes significantly changed during both NPF events and BB-UPB episodes. During the typical NPF events, the hydrophilic mode particles dominated, representing almost 80% of the total sampled particles, as marked in Fig. 5. In contrast, the hydrophobic mode particles, which accounted for 60–70% of 50-, 100-, and 250-nm particles, became more pronounced during the BB-UPB events. This finding was consistent with the chemical composition measurements, showing that the biomass-burning aerosols mainly consisted of organics and soot, which are initially hydrophobic. Bougiatioti et al. (2016) observed that the particles influenced by biomass burning in the eastern Mediterranean exhibited two different hygroscopic modes, and hydrophilic mode particles dominated. In their study, the distinct modes were not observed for the cases with a longer processing time, which allowed for condensation growth and mixing of the populations.

As listed in the Table 1, the mean overall κ values of biomass-burning aerosols during the BB-UPB events were 0.09 ± 0.04, 0.09 ± 0.02, 0.10 ± 0.03, and 0.10 ± 0.04 for 50-, 100-, 150-, and 250-nm particles, respectively (the GF-PDF of the 150-nm particles is not shown in Fig. 5). The water solubility of the biomass-burning aerosols was significantly lower than that of typical urban aerosols (κ = 0.16–0.28) in Beijing during the summertime (Wu et al., 2016). In addition, Kreidenweis and Asa-Awuku (2014) compiled the existing reports on particle hygroscopic growth described in the literature. They reported that biomass-burning aerosols typically have low hygroscopicity. For example, the almost hydrophobic and less hygroscopic modes of biomass-burning aerosols

Please cite this article as: Wu, Z., et al., Chemical and physical properties of biomass burning aerosols and their CCN activity: A case study in Beijing, China, Sci Total Environ (2016), http://dx.doi.org/10.1016/j.scitotenv.2016.11.112

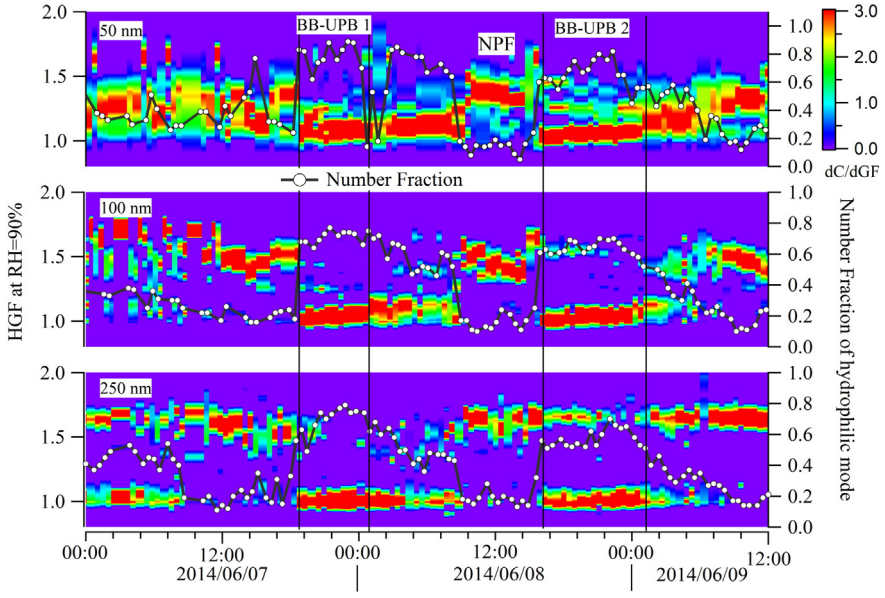

Fig. 5. Size dependence of the hygroscopic growth factor (HGF) at a relative humidity (RH) of 90% and the number fraction of hydrophilic mode particles. BB-UPB 1 and BB-UPB 2 indicate biomass burning-ultrafine particle burst events 1 and 2, respectively. NPF indicates new particle formation.

in Amazonia had κ values of 0–0.04 and 0.06–0.13, respectively (also refer to Swietlicki et al., 2008). Moreover, the κ values of biomass-burning aerosols in Brazil and the African savannah are reported to be 0.1 (also refer to Magi and Hobbs, 2003) and 0.05–0.1 (also refer to Kotchenruther and Hobbs, 1998), respectively. Similarly, Engelhart et al. (2012) have reported that the κ for biomass-burning secondary organic aerosols was 0.11, on average. These observations agreed well with our study. In contrast, Rose et al. (2010) observed that the average κ value dropped to 0.2 during a strong local biomass-burning event near the mega-city Guangzhou, China; this κ value can be considered as characteristic for freshly emitted smoke from the burning of agricultural waste. Of note, the properties of biomass-burning aerosols vary with the fuel type, combustion phase, environmental conditions, and processing (Bond et al., 2013; Vakkari et al., 2014).

During the course of the BB-UPB episode, changes in the hygroscopic growth and particle number fraction of hydrophobic mode were insignificant. This observation was consistent with the changes in the O:C ratio displayed in Fig. 2c. Thus, no obvious aging process for biomass-burning aerosols was observed. Previous studies have shown large potential changes in the size distribution, hygroscopicity, and chemical composition of biomass-burning particles during their atmospheric transport (Engelhart et al., 2012; Reid et al., 2005; Vakkari et al., 2014). For instance, photochemical processing reduces the hygroscopicity of biomass-burning particles due to the condensation of secondary organic aerosols (Engelhart et al., 2012). In our observations, the BB-UPB episodes took place in the late afternoon and lasted throughout the night. Aging in the dark may not lead to a significant change in particle hygroscopicity (Li et al., 2015).

Table 1
The hygroscopicity parameter value (κ) and number fraction (NF) of the hydrophobic mode of size-resolved biomass-burning aerosols.

Particle diameter (nm)	κ	NF
50	0.09 ± 0.04	0.70 ± 0.16
100	0.09 ± 0.02	0.66 ± 0.06
150	0.10 ± 0.03	0.60 ± 0.07
250	0.10 ± 0.04	0.62 ± 0.07

3.4. CCN activity of biomass-burning aerosols

The CCN activity of ultrafine particles during biomass-burning episodes was examined. The average κ_{CCNc} values during the biomass-burning episodes were 0.09 ± 0.03 (D_{50} = 171 ± 16 nm), 0.06 ± 0.01 (D_{50} = 118 ± 6 nm), and 0.09 ± 0.01 (D_{50} = 67 ± 3 nm) for SS = 0.2%, 0.4%, and 0.8%, respectively. The comparisons among the size-resolved κ_{HTDMA} and κ_{CCNc} values as well as the mass fraction of chemical components during the BB-UPB episodes are displayed in Fig. 6, showing that the κ_{HTDMA} value is consistent with the κ_{CCNc} value. A large discrepancy between κ values derived from HTDMA and CCNc was not observed. This observation is different from several previous studies, which have reported inconsistencies between κ_{HTDMA} and κ_{CCNc} values (Cerully et al., 2011; Good et al., 2010; Irwin et al., 2010; Petters et al., 2009b; Wex et al., 2009). The effective particle hygroscopicity (κ_{chem}) estimated from the particle chemical composition can simply be represented as a function of AMS-based organic (MF_{org}) and inorganic (MF_{irorg}) mass fractions (Gunthe et al., 2009):

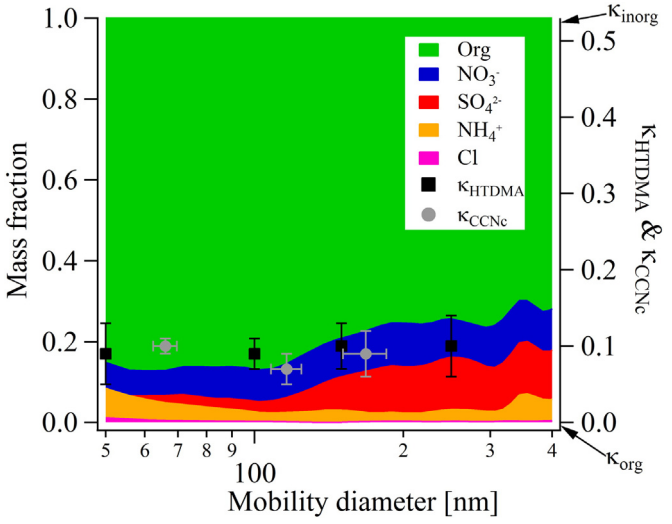

Fig. 6. Size-resolved κ_{HTDMA} and κ_{CCNc} values and the mass fraction of chemical components during the biomass burning-ultrafine particle burst event episodes.

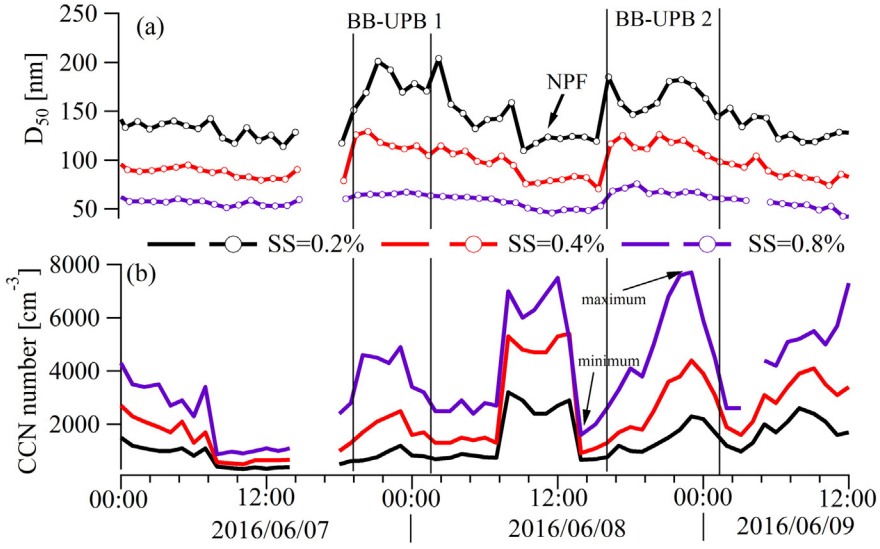

Fig. 7. The time course of the critical diameter at which 50% of the particles are activated at supersaturation (D_{50}) and the cloud condensation nuclei (CCN) number. SS, supersaturation; BB-UPB 1, biomass burning-ultrafine particle burst event 1; BB-UPB 2, biomass burning-ultrafine particle burst event 2; NPF, new particle formation.

$\kappa_{chem} = \kappa_{org} \times MF_{org} + \kappa_{inorg} \times MF_{inorg}$. Here, the density of the inorganic component was assumed to be the same as that of the organic component. In addition, κ_{inorg} is the κ value of the inorganic fraction and taken as 0.53 (ammonium sulfate) (Petters and Kreidenweis, 2007), which is the value of the upper limit of the right-hand y-axis (the pure inorganic fraction). Meanwhile, κ_{org} is the κ value of the organic fraction and is considered as 0, which is the value of the lower limit of the right-hand y-axis (the pure organic fraction). As displayed in Fig. 6, the κ_{HTDMA} and κ_{CCNc} values corresponded to the ratio of the organic and inorganic fractions with increasing particle size. Thus, the κ_{HTDMA} and κ_{CCNc} values agreed well with that (κ_{chem}) estimated from the AMS data. One should keep in mind that the BC or other refractory fraction, which are not considered in Fig. 6, may cause a discrepancy between the κ_{HTDMA} and κ_{chem} values.

The low hygroscopicity of the biomass-burning aerosols indicated that the ultrafine particles associated with biomass burning were less active. Petters et al. (2009a) investigated the CCN activity of primary aerosols emitted from the combustion of 24 vegetation types originating from various regions of the United States and Asia in the laboratory. In their study, the κ values varied between 0.02 and 0.8, showing a highly variable CCN activity. In our study, the particles were less hygroscopic, and highly hygroscopic particles were not observed. Furthermore, Engelhart et al. (2012) found that the initial CCN activity of biomass-burning aerosol emissions was highly variable; in addition, after a few hours of photochemical processing, the CCN activity converged to a certain value. The measurement site in our study may have been far from the biomass-burning fire points. After atmospheric dilution and photochemical oxidation, the chemical composition of the burning aerosols might become more homogenous. For example, KCl can change to K_2SO_4 or KNO_3, and the organics and BC concentrations can be enhanced in the individual particles (Li et al., 2010). As a result, the κ values of the biomass-burning aerosols decreased and became more identical.

The time course of D_{50} and the CCN count at SS = 0.2%, 0.4%, and 0.8% are shown in Fig. 7. Clearly, the D_{50} at each SS increased during the BB-UPB events, indicating that the biomass-burning aerosols had less active CCN compared to other types of aerosols, especially the newly formed particles during the NPF event. The CCN count increased considerably, regardless of their size during the BB-UPB events. Rose et al. (2010) also observed an increase in CCN during a biomass-burning event near the megacity of Guangzhou, China, where the CCN count was determined at Supersaturation = 0.068% and 0.27%, respectively. As shown in Fig. 2, there was a wet deposition, which removed the pre-existing particle significantly before the start of BB-UPB 2. This means that the increase in CCN count was mainly caused by biomass burning. The ratios of the maximum CCN number (marked as "maximum" in Fig. 7) during the biomass-burning events and the minimum CCN number (marked as "minimum" in Fig. 7) before the biomass-burning event are presented as the upper limit for the biomass-burning effects on CCN. The ratios for SS = 0.2%, 0.4%, and 0.8% were 4.8, 4.8, and 3.4, respectively.

4. Summary and conclusion

The NCP is the major region for planting winter wheat in China. After winter wheat is harvested, the burning of straw waste in the field inputs significant amounts of aerosol particles and trace gases into the atmosphere, giving rise to a deteriorated air quality that causes adverse effects on human health in adjacent cities. An intensive campaign was carried out in Beijing, China, in June 2014. Meanwhile, two biomass-burning events associating with increasing BC, organics, CO, and f_{60} were observed in the atmosphere of Beijing. During the biomass-burning episodes, bursts in the number of Aitken mode particles were observed. The ultrafine particles continuously grew, with growth rates of 3.9 nm/h and 6.5 nm/h, respectively. During the particle growth process, the O:C ratio, which averaged 0.23 ± 0.04, did not show an obvious enhancement, indicating that no significant aging of biomass-burning aerosols occurred during the events. On average, the organics and BC accounted for 60 ± 10% and 18 ± 3% of PM_1 (here, PM1 means the sum of NR-PM_1 and BC mass concentrations) during the BB-UPB episodes. The dominance of organics and BC evidently decreased the particle hygroscopicity. The mean overall κ values of the biomass-burning aerosols derived from both HTDMA and CCNc measurements during the BB-UPB events were approximately 0.1, regardless of the particle size. Comparisons among HGF-derived, CCN-derived, and AMS-based κ values were consistent for the biomass-burning aerosols. The low hygroscopicity (κ = 0.1) and high organic fraction (around 60%) resulted in less active CCN. In addition, the CCN count increased considerably at SS = 0.2%, 0.4%, and 0.8%.

Acknowledgments

This work was supported by the following agencies: National Natural Science Foundation of China (91544214, 21190052, 41121004, and 41475127), National Basic Research Program of China (2013CB228503), Special Fund of the State Key Joint Laboratory of

Environment Simulation and Pollution Control (14L02ESPC), the non-profit research projects of the Ministry of Environmental Protection, The People's Republic of China (201409010), and the Collaborative Innovation Center for Regional Environmental Quality. Great thanks to Mr. Ying Chen for useful discussions.

References

Adler, G., Flores, J.M., Abo Riziq, A., Borrmann, S., Rudich, Y., 2011. Chemical, physical, and optical evolution of biomass burning aerosols: a case study. Atmos. Chem. Phys. 11, 1491–1503.

Andreae, M.O., Merlet, P., 2001. Emission of trace gases and aerosols from biomass burning. Glob. Biogeochem. Cycles 15, 955–966.

Andreae, M.O., Rosenfeld, D., 2008. Aerosol–cloud–precipitation interactions. Part 1. The nature and sources of cloud-active aerosols. Earth Sci. Rev. 89, 13–41.

Arnott, P., Moosmüller, H., Fred Rogers, C., Jin, T., Bruch, R., 1999. Photoacoustic spectrometer for measuring light absorption by aerosol: instrument description. Atmos. Environ. 33, 2845–2852.

Bond, T.C., Doherty, S.J., Fahey, D.W., Forster, P.M., Berntsen, T., DeAngelo, B.J., Flanner, M.G., Ghan, S., Kärcher, B., Koch, D., Kinne, S., Kondo, Y., Quinn, P.K., Sarofim, M.C., Schultz, M.G., Schulz, M., Venkataraman, C., Zhang, H., Zhang, S., Bellouin, N., Guttikunda, S.K., Hopke, P.K., Jacobson, M.Z., Kaiser, J.W., Klimont, Z., Lohmann, U., Schwarz, J.P., Shindell, D., Storelvmo, T., Warren, S.G., Zender, C.S., 2013. Bounding the role of black carbon in the climate system: a scientific assessment. J. Geophys. Res. Atmos. 118, 5380–5552.

Bougiatioti, A., Stavroulas, I., Kostenidou, E., Zarmpas, P., Theodosi, C., Kouvarakis, G., Canonaco, F., Prévôt, A.S.H., Nenes, A., Pandis, S.N., Mihalopoulos, N., 2014. Processing of biomass-burning aerosol in the eastern Mediterranean during summertime. Atmos. Chem. Phys. 14, 4793–4807.

Bougiatioti, A., Bezantakos, S., Stavroulas, I., Kalivitis, N., Kokkalis, P., Biskos, G., Mihalopoulos, N., Papayannis, A., Nenes, A., 2016. Biomass-burning impact on CCN number, hygroscopicity and cloud formation during summertime in the eastern Mediterranean. Atmos. Chem. Phys. 16, 7389–7409.

Canagaratna, M.R., Jayne, J.T., Jimenez, J.L., Allan, J.D., Alfarra, M.R., Zhang, Q., Onasch, T.B., Drewnick, F., Coe, H., Middlebrook, A., Delia, A., Williams, L.R., Trimborn, A.M., Northway, M.J., DeCarlo, P.F., Kolb, C.E., Davidovits, P., Worsnop, D.R., 2007. Chemical and microphysical characterization of ambient aerosols with the aerodyne aerosol mass spectrometer. Mass Spectrom. Rev. 26, 185–222.

Canagaratna, M.R., Jimenez, J.L., Kroll, J.H., Chen, Q., Kessler, S.H., Massoli, P., Hildebrandt Ruiz, L., Fortner, E., Williams, L.R., Wilson, K.R., Surratt, J.D., Donahue, N.M., Jayne, J.T., Worsnop, D.R., 2015. Elemental ratio measurements of organic compounds using aerosol mass spectrometry: characterization, improved calibration, and implications. Atmos. Chem. Phys. 15, 253–272.

Capes, G., Johnson, B., McFiggans, G., Williams, P.I., Haywood, J., Coe, H., 2008. Aging of biomass burning aerosols over West Africa: aircraft measurements of chemical composition, microphysical properties, and emission ratios. J. Geophys. Res. Atmos. 113, D00C15.

Cerully, K.M., Raatikainen, T., Lance, S., Tkacik, D., Tiitta, P., Petäjä, T., Ehn, M., Kulmala, M., Worsnop, D.R., Laaksonen, A., Smith, J.N., Nenes, A., 2011. Aerosol hygroscopicity and CCN activation kinetics in a boreal forest environment during the 2007 EUCAARI campaign. Atmos. Chem. Phys. 11, 12369–12386.

Chen, Y., Bond, T.C., 2010. Light absorption by organic carbon from wood combustion. Atmos. Chem. Phys. 10, 1773–1787.

Chen, Q., Li, Y.L., McKinney, K.A., Kuwata, M., Martin, S.T., 2012. Particle mass yield from β-caryophyllene ozonolysis. Atmos. Chem. Phys. 12, 3165–3179.

Cheng, Y., Engling, G., He, K.B., Duan, F.K., Ma, Y.L., Du, Z.Y., Liu, J.M., Zheng, M., Weber, R.J., 2013. Biomass burning contribution to Beijing aerosol. Atmos. Chem. Phys. 13, 7765–7781.

Corrigan, A.L., Russell, L.M., Takahama, S., Äijälä, M., Ehn, M., Junninen, H., Rinne, J., Petäjä, T., Kulmala, M., Vogel, A.L., Hoffmann, T., Ebben, C.J., Geiger, F.M., Chhabra, P., Seinfeld, J.H., Worsnop, D.R., Song, W., Auld, J., Williams, J., 2013. Biogenic and biomass burning organic aerosol in a boreal forest at Hyytiälä, Finland, during HUMPPA-COPEC 2010. Atmos. Chem. Phys. 13, 12233–12256.

Cubison, M.J., Ortega, A.M., Hayes, P.L., Farmer, D.K., Day, D., Lechner, M.J., Brune, W.H., Apel, E., Diskin, G.S., Fisher, J.A., Fuelberg, H.E., Hecobian, A., Knapp, D.J., Mikoviny, T., Riemer, D., Sachse, G.W., Sessions, W., Weber, R.J., Weinheimer, A.J., Wisthaler, A., Jimenez, J.L., 2011. Effects of aging on organic aerosol from open biomass burning smoke in aircraft and laboratory studies. Atmos. Chem. Phys. 11, 12049–12064.

DeCarlo, P.F., Kimmel, J.R., Trimborn, A., Northway, M.J., Jayne, J.T., Aiken, A.C., Gonin, M., Fuhrer, K., Horvath, T., Docherty, K.S., Worsnop, D.R., Jimenez, J.L., 2006. Field-deployable, high-resolution, time-of-flight aerosol mass spectrometer. Anal. Chem. 78, 8281–8289.

Deng, Z.Z., Zhao, C.S., Ma, N., Liu, P.F., Ran, L., Xu, W.Y., Chen, J., Liang, Z., Liang, S., Huang, M.Y., Ma, X.C., Zhang, Q., Quan, J.N., Yan, P., Henning, S., Mildenberger, K., Sommerhage, E., Schäfer, M., Stratmann, F., Wiedensohler, A., 2011. Size-resolved and bulk activation properties of aerosols in the North China Plain. Atmos. Chem. Phys. 11, 3835–3846.

Duan, F., Liu, X., Yu, T., Cachier, H., 2004. Identification and estimate of biomass burning contribution to the urban aerosol organic carbon concentrations in Beijing. Atmos. Environ. 38, 1275–1282.

Engelhart, G.J., Hennigan, C.J., Miracolo, M.A., Robinson, A.L., Pandis, S.N., 2012. Cloud condensation nuclei activity of fresh primary and aged biomass burning aerosol. Atmos. Chem. Phys. 12, 7285–7293.

Good, N., Topping, D.O., Allan, J.D., Flynn, M., Fuentes, E., Irwin, M., Williams, P.I., Coe, H., McFiggans, G., 2010. Consistency between parameterisations of aerosol hygroscopicity and CCN activity during the RHaMBLe discovery cruise. Atmos. Chem. Phys. 10, 3189–3203.

Gunthe, S.S., King, S.M., Rose, D., Chen, Q., Roldin, P., Farmer, D.K., Jimenez, J.L., Artaxo, P., Andreae, M.O., Martin, S.T., Pöschl, U., 2009. Cloud condensation nuclei in pristine tropical rainforest air of Amazonia: size-resolved measurements and modeling of atmospheric aerosol composition and CCN activity. Atmos. Chem. Phys. 9, 7551–7575.

Gysel, M., McFiggans, G.B., Coe, H., 2009. Inversion of tandem differential mobility analyser (TDMA) measurements. J. Aerosol Sci. 40, 134–151.

He, L.-Y., Lin, Y., Huang, X.-F., Guo, S., Xue, L., Su, Q., Hu, M., Luan, S.-J., Zhang, Y.H., 2010. Characterization of high-resolution aerosol mass spectra of primary organic aerosol emissions from Chinese cooking and biomass burning. Atmos. Chem. Phys. 10: 11535–11543. http://dx.doi.org/10.5194/acp-10-11535-2010.

Hennigan, C.J., Westervelt, D.M., Riipinen, I., Engelhart, G.J., Lee, T., Collett, J.L., Pandis, S.N., Adams, P.J., Robinson, A.L., 2012. New particle formation and growth in biomass burning plumes: an important source of cloud condensation nuclei. Geophys. Res. Lett. 39, L09805.

Irwin, M., Good, N., Crosier, J., Choularton, T.W., McFiggans, G., 2010. Reconciliation of measurements of hygroscopic growth and critical supersaturation of aerosol particles in central Germany. Atmos. Chem. Phys. 10, 11737–11752.

Jung, J., Lee, S., Kim, H., Kim, D., Lee, H., Oh, S., 2014. Quantitative determination of the biomass-burning contribution to atmospheric carbonaceous aerosols in Daejeon, Korea, during the rice-harvest period. Atmos. Environ. 89, 642–650.

Kostenidou, E., Pathak, R.K., Pandis, S.N., 2007. An algorithm for the calculation of secondary organic aerosol density combining AMS and SMPS data. Aerosol Sci. Technol. 41, 1002–1010.

Kotchenruther, R.A., Hobbs, P.V., 1998. Humidification factors of aerosols from biomass burning in Brazil. J. Geophys. Res. Atmos. 103, 32081–32089.

Kreidenweis, S.M., Asa-Awuku, A., 2014. 5.13 - aerosol hygroscopicity: particle water content and its role in atmospheric processes. In: Turekian, H.D.H.K. (Ed.), Treatise on Geochemistry (Second Edition). Elsevier, Oxford, pp. 331–361.

Li, L., Wang, Y., Zhang, Q., Li, J., Yang, X., Jin, J., 2008. Wheat straw burning and its associated impacts on Beijing air quality. Sci. China Ser. D Earth Sci. 51, 403–414.

Li, W.J., Shao, L.Y., Buseck, P.R., 2010. Haze types in Beijing and the influence of agricultural biomass burning. Atmos. Chem. Phys. 10, 8119–8130.

Li, C., Ma, Z., Chen, J., Wang, X., Ye, X., Wang, L., Yang, X., Kan, H., Donaldson, D.J., Mellouki, A., 2015. Evolution of biomass burning smoke particles in the dark. Atmos. Environ. 120, 244–252.

Magi, B.I., Hobbs, P.V., 2003. Effects of humidity on aerosols in southern Africa during the biomass burning season. J. Geophys. Res. Atmos. 108 (n/a-n/a).

Massling, A., Wiedensohler, A., Busch, B., Neusüß, C., Quinn, P., Bates, T., Covert, D., 2003. Hygroscopic properties of different aerosol types over the Atlantic and Indian Oceans. Atmos. Chem. Phys. 3, 1377–1397.

Massling, A., Niedermeier, N., Hennig, T., Fors, E.O., Swietlicki, E., Ehn, M., Hämeri, K., Villani, P., Laj, P., Good, N., McFiggans, G., Wiedensohler, A., 2011. Results and recommendations from an intercomparison of six hygroscopicity-TDMA systems. Atmos. Meas. Tech. 4, 485–497.

Mukai, S., Yasumoto, M., Nakata, M., 2014. Estimation of biomass burning influence on air pollution around Beijing from an aerosol retrieval model. ScientificWorldJournal 2014, 649648.

Petters, M.D., Kreidenweis, S.M., 2007. A single parameter representation of hygroscopic growth and cloud condensation nucleus activity. Atmos. Chem. Phys. 7, 1961–1971.

Petters, M.D., Carrico, C.M., Kreidenweis, S.M., Prenni, A.J., DeMott, P.J., Collett Jr., J.L., Moosmüller, H., 2009a. Cloud condensation nucleation activity of biomass burning aerosol. J. Geophys. Res. 114, D22205.

Petters, M.D., Wex, H., Carrico, C.M., Hallbauer, E., Massling, A., McMeeking, G.R., Poulain, L., Wu, Z., Kreidenweis, S.M., Stratmann, F., 2009b. Towards closing the gap between hygroscopic growth and activation for secondary organic aerosol – part 2: theoretical approaches. Atmos. Chem. Phys. 9, 3999–4009.

Reid, J.S., Koppmann, R., Eck, T.F., Eleuterio, D.P., 2005. A review of biomass burning emissions part II: intensive physical properties of biomass burning particles. Atmos. Chem. Phys. 5, 799–825.

Roberts, G.C., Nenes, A., 2005. A continuous-flow streamwise thermal-gradient CCN chamber for atmospheric measurements. Aerosol Sci. Technol. 39, 206–221.

Robinson, A.L., Grieshop, A.P., Donahue, N.M., Hunt, S.W., 2010. Updating the conceptual model for fine particle mass emissions from combustion systems. J. Air Waste Manage. Assoc. 60, 1204–1222.

Rose, D., Nowak, A., Achtert, P., Wiedensohler, A., Hu, M., Shao, M., Zhang, Y., Andreae, M.O., Pöschl, U., 2010. Cloud condensation nuclei in polluted air and biomass burning smoke near the mega-city Guangzhou, China – part 1: size-resolved measurements and implications for the modeling of aerosol particle hygroscopicity and CCN activity. Atmos. Chem. Phys. 10, 3365–3383.

Saleh, R., Robinson, E.S., Tkacik, D.S., Ahern, A.T., Liu, S., Aiken, A.C., Sullivan, R.C., Presto, A.A., Dubey, M.K., Yokelson, R.J., Donahue, N.M., Robinson, A.L., 2014. Brownness of organics in aerosols from biomass burning linked to their black carbon content. Nat. Geosci. 7, 647–650.

Spracklen, D.V., Carslaw, K.S., Pöschl, U., Rap, A., Forster, P.M., 2011. Global cloud condensation nuclei influenced by carbonaceous combustion aerosol. Atmos. Chem. Phys. 11, 9067–9087.

Swietlicki, E., Hansson, H.C., HÄMeri, K., Svenningsson, B., Massling, A., McFiggans, G., McMurry, P.H., PetÄJÄ, T., Tunved, P., Gysel, M., Topping, D., Weingartner, E., Baltensperger, U., Rissler, J., Wiedensohler, A., Kulmala, M., 2008. Hygroscopic properties of submicrometer atmospheric aerosol particles measured with H-TDMA instruments in various environments—a review. Tellus Ser. B Chem. Phys. Meteorol. 60, 432–469.

Please cite this article as: Wu, Z., et al., Chemical and physical properties of biomass burning aerosols and their CCN activity: A case study in Beijing, China, Sci Total Environ (2016), http://dx.doi.org/10.1016/j.scitotenv.2016.11.112

Trentmann, J., Andreae, M.O., Graf, H.-F., 2003. Chemical processes in a young biomass-burning plume. J. Geophys. Res. Atmos. 108 (n/a-n/a).

Vakkari, V., Kerminen, V.-M., Beukes, J.P., Tiitta, P., van Zyl, P.G., Josipovic, M., Venter, A.D., Jaars, K., Worsnop, D.R., Kulmala, M., Laakso, L., 2014. Rapid changes in biomass burning aerosols by atmospheric oxidation. Geophys. Res. Lett. 41, 2644–2651.

Wang, L., Xin, J., Li, X., Wang, Y., 2015. The variability of biomass burning and its influence on regional aerosol properties during the wheat harvest season in North China. Atmos. Res. 157, 153–163.

Wex, H., Petters, M.D., Carrico, C.M., Hallbauer, E., Massling, A., McMeeking, G.R., Poulain, L., Wu, Z., Kreidenweis, S.M., Stratmann, F., 2009. Towards closing the gap between hygroscopic growth and activation for secondary organic aerosol: part 1 – evidence from measurements. Atmos. Chem. Phys. 9, 3987–3997.

Wu, Z.J., Hu, M., Liu, S., Wehner, B., Bauer, S., Ma ßling, A., Wiedensohler, A., Petäjä, T., Dal Maso, M., Kulmala, M., 2007. New particle formation in Beijing, China: statistical analysis of a 1-year data set. J. Geophys. Res. Atmos. 112, 797–806.

Wu, Z.J., Nowak, A., Poulain, L., Herrmann, H., Wiedensohler, A., 2011. Hygroscopic behavior of atmospherically relevant water-soluble carboxylic salts and their influence on the water uptake of ammonium sulfate. Atmos. Chem. Phys. 11, 12617–12626.

Wu, Z.J., Zheng, J., Shang, D.J., Du, Z.F., Wu, Y.S., Zeng, L.M., Wiedensohler, A., Hu, M., 2016. Particle hygroscopicity and its link to chemical composition in the urban atmosphere of Beijing, China, during summertime. Atmos. Chem. Phys. 16, 1123–1138.

Zheng, X., Liu, X., Zhao, F., Duan, F., Yu, T., Cachier, H., 2005. Seasonal characteristics of biomass burning contribution to Beijing aerosol. Sci. China, Ser. B Chem. 48, 481–488.

Please cite this article as: Wu, Z., et al., Chemical and physical properties of biomass burning aerosols and their CCN activity: A case study in Beijing, China, Sci Total Environ (2016), http://dx.doi.org/10.1016/j.scitotenv.2016.11.112